Eur. Phys. J. A **3**, 75–83 (1998)

THE EUROPEAN PHYSICAL JOURNAL A

Thermal multifragmentation in p + Au interactions at 2.16, 3.6 and 8.1 GeV incident energies

S.P. Avdeyev[1], V.A. Karnaukhov[1], W.D. Kuznetsov[1], L.A. Petrov[1], V.K. Rodionov[1], A.S. Zubkevich[1], H. Oeschler[2], O.V. Bochkarev[3], L.V. Chulkov[3], E.A. Kuzmin[3], A. Budzanovski[4], W. Karcz[4], M. Janicki[4], E. Norbeck[5], A.S. Botvina[6,7], W.A. Friedman[8], W. Nörenberg[9], G. Papp[9]

[1] Joint Institute for Nuclear Research, 141980, Dubna, Russia
[2] Institut für Kernphysik, Technische Universität Darmstadt, 64289 Darmstadt, Germany
[3] Kurchatov Institute, 123182 Moscow, Russia
[4] H. Niewodniczanski Institute of Nuclear Physics, 31-342, Cracow, Poland
[5] University of Iowa, Iowa City, IA 52242, USA
[6] INFN and Dipartimento di Fisica, 40126 Bologna, Italy
[7] Institute for Nuclear Research, 117312, Moscow, Russia
[8] Physics Department, University of Wisconsin, Madison, Wisconsin 53706, USA
[9] Gesellschaft für Schwerionenforschung, D-64291 Darmstadt, Germany

Received: 15 December 1997 / Revised version: 24 April 1998
Communicated by V. Metag

Abstract. Multiple emission of intermediate-mass fragments has been studied for the collisions p + Au at 2.16, 3.6 and 8.1 GeV with the FASA setup. The mean IMF multiplicities for events with at least one IMF are equal to 1.7, 1.9 and 2.1 (±0.2) respectively. The multiplicity, charge distributions and kinetic energy spectra of IMF are described in the framework of a intranuclear cascade model followed by the statistical multifragmentation model. However, between the two parts of the calculation the excitation energies and the residual masses and charges are modified to take into account the losses during expansion. The results support a scenario of true thermal multifragmentation of a hot and expanded target spectator.

PACS. 25.70.Pq Multifragment emission and correlations – 25.70.Mn Projectile and target fragmentation – 25.40.Ve Other reactions above meson production thresholds (energies >400 MeV)

1 Introduction

The investigation of the decay of very hot nuclei has become a topic of great interest. It is largely concentrated on the process of multiple emission of intermediate mass fragments (IMF, $3 \leq Z \leq 20$) [1-3]. Now, it is established as the main decay mode of highly excited nuclei, and this process is likely to occur when a nucleus has expanded and lower density is reached. It is under debate whether this process is related to a liquid-gas phase transition in nuclear matter [4]. A common way to produce very hot nuclei is to use reactions induced by heavy ions at energies 30–100 MeV/nucleon. But in this case heating is accompanied by compression, strong rotation and shape distortion, which cause dynamic effects in the nuclear decay. It seems difficult to disentangle all these influences to extract information on the thermodynamic properties of a hot nuclear system. The situation becomes clearer when light relativistic projectiles are used [5-12]. One expects that dynamic effects are negligible in that case. A similar situation is achieved by the abrasion mechanism in heavy-ion collisions [13]. An advantage of light-ion bombardment is that all the IMF's are emitted by one source only – the target spectator. A crucial point in these studies is whether sufficient excitation energy is reached to induce a significant yield of IMF production [6].

The time scale of IMF emission is a key characteristic for understanding this decay process: Is it a "slow" sequential process of independent emission of IMF's or is it a new decay mode with "simultaneous" ejection of the fragments governed by the total accessible phase space? Usually, only the latter process is called "multifragmentation". "Simultaneous" means that all fragments are liberated during a time which is smaller than a characteristic Coulomb time t_c of $\approx 10^{-21}$ s [14]. For that case emission of IMF's is not independent, they interact via long-range Coulomb forces during acceleration in the electrical field after freeze-out. Measurement of the emission time for IMF's (i.e. the mean time between two consecutive fragment emissions) is a direct way to answer the question as to the nature of the multifragmentation phenomenon. By studying the relative angle IMF-IMF correlations we

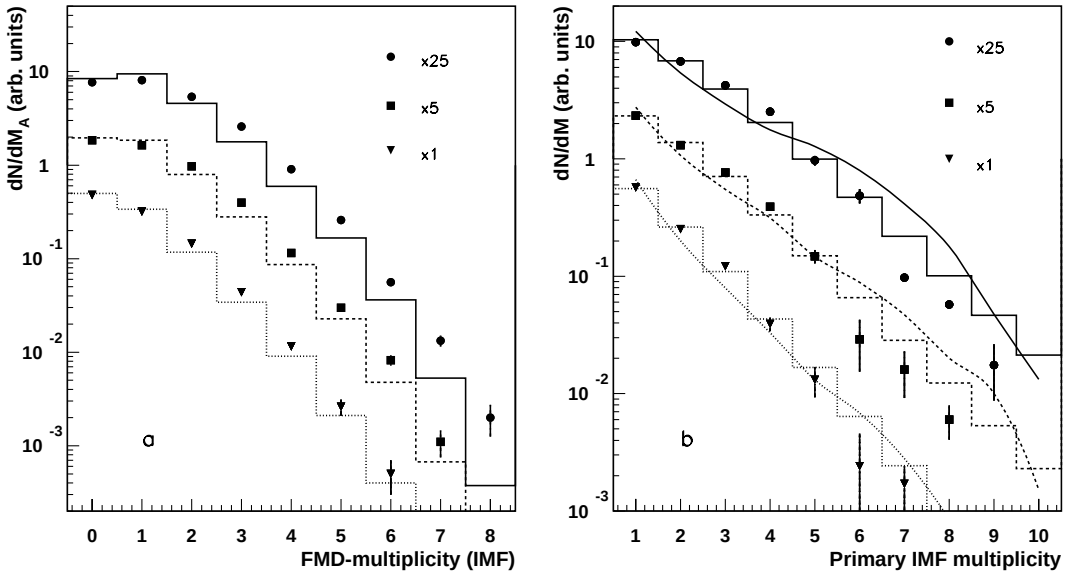

Fig. 1. a Measured IMF-multiplicity distributions (symbols) and fits with a Fermi distribution (folded with the experimental filter, histograms) associated with a trigger fragment for p + Au collisions at 8.1 GeV (circles, solid line), 3.6 GeV (squares, dashed line), 2.16 GeV (triangles, dotted line), **b** Symbols (same notation as in the upper part) represent directly reconstructed primary IMF distributions; Histograms are the Fermi distributions used to fit the data in the upper part. The smooth lines are calculated with the statistical multifragmentation model (see text)

found that for ^{4}He+Au collisions at 14.6 GeV the emission time is less than $3 \cdot 10^{-22}$ s (100 fm/c) [15,16].

In this paper we present the experimental study of multifragment emission induced by relativistic protons (up to 8.1 GeV) on gold. Properties of the emitted IMF's, i.e. their multiplicities, energy, charge and angular distributions are presented and compared to intranuclear cascade calculations followed by statistical decay. A short presentation of the data was given in [17]. We emphasize a shortcoming of this two-step mechanism by discussing the influence of expansion before break-up. Finally, we argue whether the observed decay can be considered as "thermal multifragmentation".

2 Experimental setup

The experiments were performed with a proton beam from the JINR synchrophasotron in Dubna at energies of 2.16, 3.6 and 8.1 GeV using the modified [18] 4π-setup FASA [19]. The main parts of the device are: (i) five ΔE (ionisation chambers) $\times$ E (Si)-telescopes, which serve as a trigger for the read-out of the system allowing measurement of the charge and energy distributions of IMF's at different angles. They are located at $\theta = 24°$, $68°$, $87°$, $112°$ and $156°$ to the beam direction and together cover a solid angle of 0.03 sr; (ii) a fragment multiplicity detector (FMD) consisting of 64 CsI(Tl) counters (with thicknesses around 30 mg·cm^{-2}) which covers 89% of 4π. The FMD gives the number of IMF's in the event and their spatial distribution. Their plexiglass light guides were replaced by hollow metal tubes with a diffuse reflector [18]. This results in reducing the background in the FMD (down to less than 2%) caused by the beam halo. Background was continuously controlled by means of a double-gate mode in processing the photo-multiplier pulses [19]. The scintillator faces were covered by aluminized mylar (0.2 mg·cm^{-2}) to exclude light cross-talk [18].

A self-supporting Au target 1.5 mg/cm^2 thick was located in the center of the FASA vacuum chamber. The average beam intensity was $7 \cdot 10^8$ p/spill (spill length 300 ms, spill period 10 s). The blank-target background for telescopes in the angular range $65° - 115°$ is around 5% for $Z_f = 2$ decreasing with Z_f to $\leq 1\%$ for $Z_f \geq 6$.

In this work we revised the calculations of the efficiency of IMF registration by the scintillation counters. New data on the response function of CsI(Tl) to heavy ions [20] were used and self-absorption of light in polycrystalline CsI(Tl) [19] was taken into account. The pulse-height thresholds were set off-line in each counter individually depending on the scintillator thickness to get good separation of IMF from lighter fragments ($Z = 1, 2$). The calculated efficiency of the FMD for IMF detection is $\varepsilon = 59\%$, while the admixture of lighter particles to the counting rate is less than 5% with respect to IMF's.

3 Results

3.1 Fragment multiplicity

The measured IMF-multiplicity distributions associated with a trigger fragment in one of the telescopes are shown in Fig. 1. The measured mean multiplicities do not depend significantly on the triggering condition. They vary

within 5% when the charges of the triggering fragment change from $Z \geq 3$ to $Z \geq 10$. The data were corrected for the admixture of lighter fragments and background in the FMD. It was done using the random generator procedure. The mean multiplicities measured by the FMD $< M_A >$ for the beam energies 2.16, 3.6 and 8.1 GeV are equal to 0.73, 0.96 and 1.11 respectively with an error of $\pm$ 0.02.

The measured multiplicity distribution $W_A(M_A)$ differs from the primary multiplicity distribution $W(M)$ because of distortion by triggering and because the FMD efficiency is less than 100%. These distributions are related via the response matrix of the FASA setup $Q(M_A, M)$:

$$W_A(M_A) = \sum_{M=M_A+1} Q(M_A, M) \cdot W(M) \,. \qquad (1)$$

The response matrix includes the triggering probability, which is proportional to M, and the probability of detecting (in FMD) M_A fragments from the remaining $M-1$. The latter probability is described by the binomial distribution. So, we have:

$$Q(M_A, M) \, = \, \frac{M!}{M_A!(M-1-M_A)!} \, \varepsilon^{M_A} (1-\varepsilon)^{M-1-M_A} \,, \qquad (2)$$

with ε the detection efficiency.

It is important to check the separation of IMFs from slow He ions. This is done using IMF coincidences in the trigger telescopes. From (1) and (2) one finds the following relation between $< M_A >$ and the moments of the primary multiplicity distribution:

$$\frac{< M_A >}{\varepsilon} \, = \, \frac{< M^2 >}{< M >} \, - \, 1 \,. \qquad (3)$$

This expression gives the mean IMF multiplicity for events selected by triggering. The right side of this equation can be obtained also from the coincidence rate n_{12} for IMF in the triggering telescopes:

$$\frac{n_{12}}{n_1 p_2} \, = \, \frac{< M^2 >}{< M >} \, - \, 1 \,. \qquad (4)$$

Here n_1 is counting rate in telescope 1, p_2 is the detection probability for the coincident fragment in telescope 2.

We used the coincidence data for the telescopes located at θ equal to 68°, 87° and 112°. For that geometry the probability p_2 is largely determined by the solid angle of telescope 2. The correction for the IMF-IMF angular correlation is around 6%. The values of ($< M^2 > / < M > -1$) determined from the coincidence rates and from the FMD array differ by 7%, and that is within the counting-rate statistics of coincidences. Therefore, an error of 10% has been taken for the mean primary IMF multiplicities caused by He admixtures and uncertainties in the efficiency determination of the FMD array.

To obtain the primary multiplicity distribution $W(M)$ from the measured one $W_A(M_A)$ there are two options. The first is to fit the parametrized $W(M)$, folded by the experimental filter according to (1), to the experimental distribution. It was done assuming $W(M)$ to be shaped like a Fermi function. This choice was motivated by calculations using the statistical model of multifragmentation (see below). The results are presented in Fig. 1. The mean values of the primary IMF multiplicities (for the events with at least one IMF) are equal to 1.7±0.2, 1.9±0.2 and 2.1±0.2 for the beam energies 2.16, 3.6 and 8.1 GeV, respectively. These results are shown as points in Fig. 2 together with calculations which are discussed later. Note that these values are considerably larger than mean IMF multiplicities referring to all events. Multifragmentation of gold induced by relativistic protons is investigated in a recent paper [10]. Our results are in general agreement with those presented. But unfortunately we cannot compare directly the mean primary multiplicities as the corresponding values are not given in [10]. Our mean IMF multiplicities are in good agreement with other studies of the ISIS group [8,9].

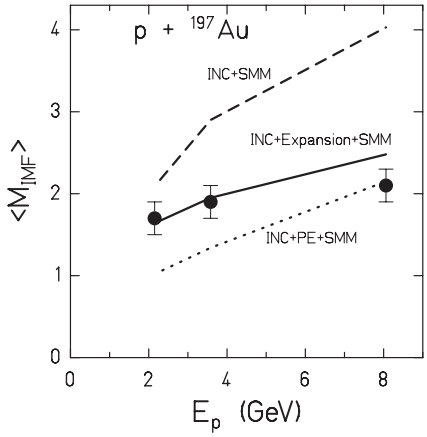

Fig. 2. Mean IMF multiplicities (for events with at least one IMF) as a function of the beam energy. The full points are experimental data. Dashed and dotted lines are drawn through the values calculated with INC+SMM and with INC+PE+SMM at the beam energies used. The solid line is obtained with the use of INC+Expansion+SMM

With the modified FASA setup we have repeated the measurements for the previously studied He + Au collisions [6]. With the updated efficiencies we obtain IMF multiplicities lower than published [6], i.e. at the incident energy of 3.6 GeV/nucleon we find 2.2±0.2 and at 1 GeV/nucleon, 2.0±0.2.

The second option is the direct reconstruction of $W(M)$ using the inverse matrix $Q^{-1}(M, M_A)$:

$$W(M) \, = \, \sum_{M_A=0}^{M-1} Q^{-1}(M, M_A) W_A(M_A) \,. \qquad (5)$$

The matrix Q^{-1} is obtained by solving the equation $Q \cdot Q^{-1} \, = \, 1$. The directly reconstructed distributions $W(M)$ are close in shape to the Fermi distributions which are shown in Fig. 1 together with the distributions calculated by the statistical multifragmentation model discussed later.

Table 1. The calculated properties of the nuclear remnants in p + Au collisions. $< M_{IMF} >$ is the total number of IMFs for events with at least one IMF. Z_R, A_R, E_R are the charge, mass number and excitation energy (in MeV) averaged over all inelastic collisions; Z_{MF}, A_{MF}, E_{MF} are the same, but averaged only over the residues which decay by IMF emission

E_p	Exper.	Calculations							Model
(GeV)	$< M_{IMF} >$	$< M_{IMF} >$	Z_R	A_R	Z_{MF}	A_{MF}	E_R	E_{MF}	
		4.03	74	180	70	169	524	880	INC+SMM
8.1	2.1±0.2	2.15	67	163	50	121	204	526	INC+PE+SMM
		2.48	71	171	63	148	279	566	INC+Expan.+SMM
		3.08	76	185	73	177	407	732	INC+SMM
3.6	1.9±0.2	1.34	70	171	55	134	148	385	INC+PE+SMM
		1.95	74	180	70	165	257	538	INC+Expan.+SMM
		2.15	77	188	75	181	328	625	INC+SMM
2.16	1.7±0.2	1.02	72	176	62	145	119	266	INC+PE+SMM
		1.64	76	185	73	176	253	527	INC+Expan.+SMM

3.2 Comparison with model calculations

The reaction mechanism for light relativistic projectiles is usually divided into two steps. The first one consists of a fast energy-deposition stage, during which very energetic light particles are emitted and the nuclear remnant (spectator) is excited. The second one is the decay of the target spectator. The fast stage is usually described by the intranuclear cascade model (INC). We use a version of the INC from [21] to get the distributions of the nuclear remnants in charge, mass and excitation energy. The second stage is described by the statistical multifragmentation model (SMM) [3,22]. The statistical behaviour of the target spectator is evident from the fact that the angular distributions of IMF's and their energy spectra at different angles are well described in the framework of the statistical decay of a thermalized moving source. This will be demonstrated in Sect. 3.3.

Within the SMM the probabilities of different decay channels are proportional to their statistical weights. The break-up volume determining the Coulomb energy of the system is taken to be $V_b = (1 + k)A/\rho_0$, where A is the mass number of the decaying nucleus, ρ_0 is the normal nuclear density, k is a model parameter. So, thermal expansion of the system before the break-up is assumed. In [6,23] we have shown that the break-up occurs at low densities. The primary fragments are hot, and their deexcitation is taken into account to get final IMF distributions. In further calculations we use $k = 2$ based on our analysis of the correlation data [16]. This value corresponds to the break-up density $\rho_b \approx \rho_0/3$. The upper dashed line in Fig. 2 is obtained by means of this combined model. The calculated mean multiplicity for the highest energy is almost two times larger than the experimental one. This might indicate a significant overestimation of the excitation energy of the residual nucleus. For the lowest beam energy the calculated mean multiplicity is still somewhat larger than the experimental one.

The use of the preequilibrium exciton model (PE) [24] together with the INC results in significantly decreasing excitation energies of the target spectator and reducing mean IMF multiplicities (lower dotted line in Fig. 2 and Table 1). The calculated value of $< M >$ at the beam energy 8.1 GeV coincides with the experimental one, but the model-predicted fragment kinetic energies are significantly lower than the measured ones (see Fig. 9). This means that the model underestimates the Z value of the target residue, as the fragment kinetic energies are determined essentially by the Coulomb field of the source [16]. With decreasing beam energy, the calculated mean IMF multiplicities fall rather fast approaching the lower limit of 1 at $E_p = 2.16$ GeV. Apparently, the PE model reduces the excitation energies of the spectators too drastically. We conclude that neither INC nor INC+PE describes the properties of a target spectator for a wide range of projectile energies. The authors of [25] came to a similar conclusion and extracted a phenomenological ensemble of the mass numbers and the excitation energies of sources to describe multifragmentation of spectators in relativistic heavy-ion reactions.

The failure of the two-stage approach suggests that additional loss of particles and energy takes place between the energy deposition and the thermal IMF production. This emission could occur during the expansion of the excited nucleus before fragment formation. Therefore, we have modified the results of the INC before starting the SMM code. In this modification the masses and charges of the residual and their excitation energies are changed, as will be discussed in the next section.

3.3 Expansion of hot nuclei

There are several models of expanding nuclei which can serve as guidelines for determining the initial parameters for the SMM calculations. We make use of the Expanding-Emitting-Source model (EES) by Friedman [26] and the expansion model (P-N) by Papp and Nörenberg [27]. Both models describe the expansion of a homogeneous sphere. The main differences of these descriptions are as follows:

– In P-N effective Skyrme interactions are used in order to describe consistently the ground-state energy and density of the initial hot nucleus, the collective

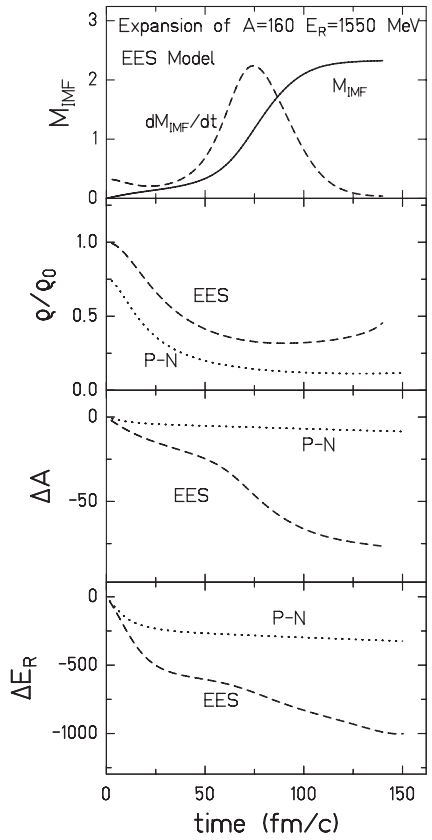

Fig. 3. Illustration of the expansion in the EES model by Friedman and the expansion model by Papp and Nörenberg (denoted P-N). In the upper part the IMF multiplicity (solid line) and their rate (dashed line, in arb. units) are shown as a function of time. The other three figures show the time evolution of the density, the loss of mass and of energy in the two models

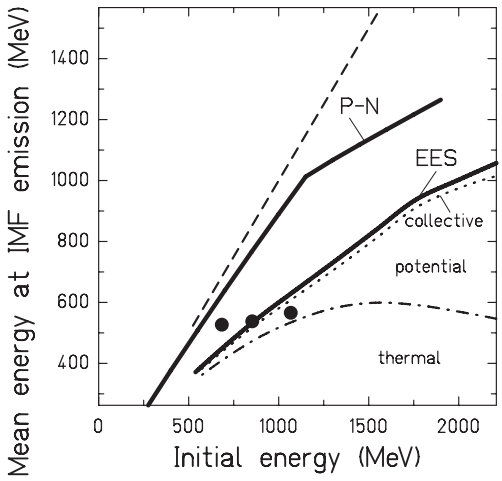

Fig. 4. The loss in excitation energy during expansion for the two models EES and P-N is compared with the empirically deduced drop from the data (for details see text). The dashed line represents the initial energy, the two solid lines the energies at break-up. For the EES model the respective contributions (collective, potential and thermal energies) are given

dynamics and the chemical potentials of protons and neutrons. In EES the expansion is obtained from a parametrization of the potential energy and the thermal pressure for a Fermi gas.

– In P-N only neutron and proton emission is considered while also complex particle emission is included in EES.

These conceptual differences show up clearly in the results shown in Fig. 3 for the expansion of the nucleus ^{160}Gd with an excitation energy of 1550 MeV. The expansion is illustrated by the time evolution of the density ρ within the homogeneous sphere. In EES the expansion starts from normal nuclear density ρ_0 and reaches the break-up density after about 75 fm/c. The mean time for emission varies little with excitation energy. Furthermore, the IMF emission in this model occurs within a time interval of 50 fm/c which agrees well with the experimental findings that the time between IMF emissions is less than 100 fm/c [15,16]. The density in P-N starts from the g.s. density of 0.76 ρ_0 for ^{160}Gd and reaches $\rho_0/3$ already after 25 fm/c. Since the matter enters the spinodal instability regime even earlier (for densities around 0.5 ρ_0), P-N assumes that clustering takes place simultaneously. It is interesting to observe that the rate of IMF emission dM_{IMF}/dt in EES becomes large only after the matter has entered the spinodal region. Due to the fast cooling of the expanding nucleus the mean number of emitted nucleons is only 3.4 in P-N until $\rho = 0.5\rho_0$ is reached. The large difference between EES and P-N in the mass emitted from the expanding nuclei during the first 30 fm/c results probably from the larger densities and temperatures in EES. It has been shown earlier [28] that for a nucleus with fixed density the rate of nucleons lost by statistical emission in the EES [29] is the same as by the evaporation code used in P-N. Furthermore, it has been checked within both models that the loss in charge proceeds in such a way that the initial N/Z ratio is essentially conserved.

It is the change in E_R and A during expansion that is suggested to be missing in the previous INC-SMM calculation. Figure 4 displays the loss in excitation energy for various initial values $E_R^{initial}$ (dashed line) until the break-up condition. The lower thick line denotes the excitation energies in the EES model at the moment when the IMF's are emitted (mean time of dM_{IMF}/dt). This remaining energy is composed of collective, potential and thermal parts as illustrated in Fig. 4. Correlated with the drop in E_R is a loss in mass. The densities at break-up vary with initial energy. The upper thick line for the P-N model is determined by the energies at the turning points of the expansion or – above the break in the curve – by the energies given at the break-up density $\rho_b = 0.3\rho_0$ when no turning point exists at large densities. This curve is expected to give an upper limit of the energy for the SMM, because additional loss of (thermal) energy stems from the emission of light particles during the growth of instabilities or from incomplete thermalization (collective flow) while going through the break-up point.

These calculations could serve as a recipe for modifying E_R, A and Z obtained from the INC before starting the SMM code. We have chosen to modify E_R empirically to obtain agreement with the measured IMF multiplicities. According to SMM the mean IMF multiplicity grows with excitation energy up to ≈ 9 MeV/nucleon and drops for higher excitation due to the transition into the vaporization regime. As in our case the excitation energies are below that limit, we introduced the parameter α as

$$\alpha = \frac{< M_{\rm exp} >}{< M_{INC+SMM} >}. \qquad (6)$$

The excitation energies E_R^{INC} given by the INC are then reduced event-by-event by applying $E_{MF} = \alpha \times E_R^{INC}$ with E_{MF} the excitaion energy at break-up. With (6) the values of α are determined as 0.77, 0.63 and 0.53 for the beam energies of 2.16, 3.6 and 8.1 GeV, respectively. Correlated with the drop in excitation energy is a loss in mass which equals $(1-\alpha) \times E_R^{INC}$. From the INC calculations we know that the nucleon losses during the cascade stage are proportional to E_R^{INC}. Therefore, we can write that the mass loss during "expansion" ΔA^* is proportional to $(1-\alpha) \times \Delta A^{INC}$. In the following we have assumed equality of these values. It corresponds to an equality of the mean excitation energy per ejected particle after the INC stage (which is around 30 MeV) and the mean energy loss per nucleon emitted during the expansion. Both expansion models support this relation as similar loss in energy per nucleon occur in these approaches.

The obtained mean values of $< E_{MF} >$ are plotted in Fig. 4 as full points. At the highest incident energy the drop is in good agreement with the predictions of the Friedman model, at the lower energies the reduction is smaller. Here the prediction of the model by Papp and Nörenberg is in better agreement with our deduced drop.

The solid curve in Fig. 2 shows the IMF multiplicities obtained with the just introduced INC+Expansion+SMM concept using the distributions of E_{MF} and A_{MF} as discussed before. This line describes the data well; in fact our procedure is a way to estimate the excitation energy when the break-up happens and is similar to earlier works [25, 30, 31].

Table 1 summarizes the results of the calculations. Note that according to the INC-Expansion-SMM model, the mean excitation energy of the residues E_R is changed only slightly with beam energy. A saturation effect in excitation energy was already noted for ^{3}He interactions (up to 4.8 GeV) with Ag [8, 9]. The IMF emission takes place on the tail of the excitation-energy distribution, therefore the mean excitation of the fragmenting nuclei is much larger.

3.4 Energy spectra, charge and angular distributions of IMF

In this chapter we study detailed properties of the outgoing fragments, i.e. their energy spectra, their angular distributions etc. in order to test whether these observations are in accordance with a thermal multifragmentation process.

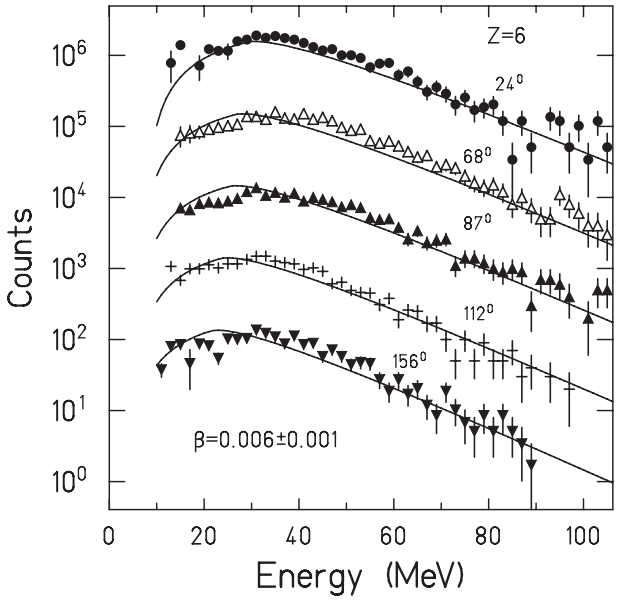

Fig. 5. Energy distribution of emitted carbon isotopes at the angles indicated for the incident energy of 8.1 GeV. The yields are multiplied by factors of ten for the presentation. The lines are fits describing isotropic emission from one source moving with $\beta = 0.006 \pm 0.001$

Figure 5 displays the energy spectra of outgoing carbon isotopes at various angles for the incident energy of 8.1 GeV. The spectra are described by an isotropic emission from a moving source using the parametrization of [32, 33]:

$$\frac{d^2\sigma}{dEd\Omega} = \frac{1}{\Delta} \int_{E_C-\Delta/2}^{E_C+\Delta/2} \frac{N}{2(\pi T)^{3/2}} \sqrt{\frac{E(E'-\epsilon)}{E'}} \times \exp\left(-\frac{E'-\epsilon}{T}\right) d\epsilon \qquad (7)$$

with N the yield, T the inverse slope parameter, E the energy in the laboratory system, E_C the Coulomb barrier, Δ the width of the distribution of the Coulomb energy. Further,

$$E' = E + E_t - 2\sqrt{E\ E_t} \quad cos\theta_{lab}$$

with $E_t = \frac{1}{2}m(c\beta)^2$ where β is the source velocity and m the fragment mass. The angle of the fragment in the lab system is θ_{lab}. Using these formulae the source velocity was determined to be $\beta = 0.006 \pm 0.001$ (without width), the Coulomb barrier to be $E_C = 16 \pm 1$ MeV using a spread of 20 MeV, and the inverse slope parameter to be $T = 14 \pm 1$ MeV.

Figure 6 presents the longitudinal versus transverse velocity plots for carbon fragments produced in p+Au collisions at 8.1 GeV. The symbols represent constant invariant cross sections taken for the fragment energy range just above the spectral peaks. These symbols are connected by circles, corresponding to the isotropic emission in the frame of a single moving source with the mean velocity

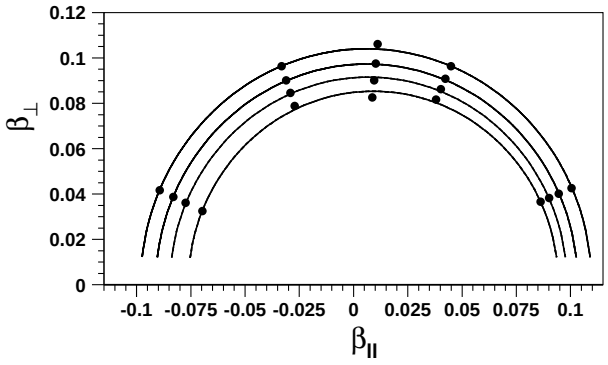

Fig. 6. Transverse versus longitudinal velocity plot for emitted carbon isotopes at 8.1 GeV. Circles are drawn through points of equal invariant cross section corresponding to isotropic emission of the fragments in the moving source frame

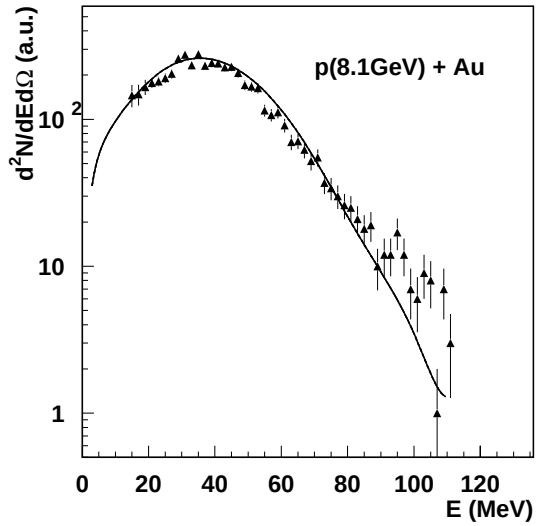

Fig. 8. Energy distribution of carbon isotopes obtained at 8.1 GeV incident energy compared to the one from the INC+Expansion+SMM calculation

(0.007-0.009) c. This value is slightly larger than the one mentioned above as in the velocity plot analysis the averaging is done only over a part of the energy spectra. The mean source velocity, predicted by the INC model is around 0.007 c.

The results observed for carbon isotopes are found also for the other fragments. This is demonstrated by the angular distributions in laboratory system given in Fig. 3.4 for outgoing fragments with $Z = 4 - 10$. They exhibit a small forward rise originating from the center-of-mass motion of the emitting source.

Finally we compare in Fig. 8 the energy spectrum of carbon fragments with the model prediction. The measured sprectrum agrees well with the INC+Expansion+SMM model in which the emission occurs at $\rho/\rho_0 = 0.3$ and the energies are only due to Coulomb repulsion and thermal motion. A contribution from collective flow is not visible yielding a limit for the flow velocity of v_{flow} is < 0.02 c. For the case of heavy ion collisions collective flow is observed and it is most pronounced in Au+Au collisions [34].

Figure 9 presents the comparison of the mean kinetic energies of fragments (measured at the beam energies 2.16 and 8.1 GeV) with the calculated ones. The data are obtained with the telescope located at $\theta = 87°$ and corrected for the detection threshold ($E/A = 1.2$ MeV). The measured mean energies for the lower beam energy are slightly higher than those for $E_p = 8.1$ GeV. This is caused by the larger charge of the decaying nucleus at the lower beam energy.

Let us first consider the region $Z_{IMF} \leq 9$. The calculations using the INC+PE+ SMM model for $E_p = 8.1$ GeV gives significantly lower mean energies than the experimental ones indicating the model underestimation of the target spectator Z and A. The calculated mean energies are close to the data when the INC+Expansion followed by SMM is used. For $Z_{IMF} > 9$ the energies do hardly change in contrast to the model prediction. We believe this observation indicates the failure of the SMM assumption that the fragments have equal probabilities to be formed at any available place inside the break-up volume. In fact, the interior of the expanded nucleus is favored over the diffuse edge for the appearance of larger IMF's as the fragments are formed via density fluctuations. This results in lower Coulomb energies for them with respect to the model prediction. This observation presents additional evidence for the volume emission of the fragments. A similar conclusion was made in [35]. An alternative explanation could be a redistribution of the total kinetic energy of the system in favour of light particles caused by fast secondary deexcitation of big IMF's during their Coulomb acceler-

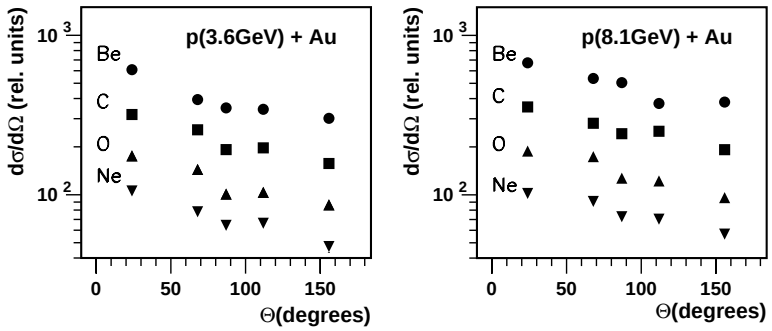

Fig. 7. Angular distributions in the laboratory system of emitted fragments from Be to Ne

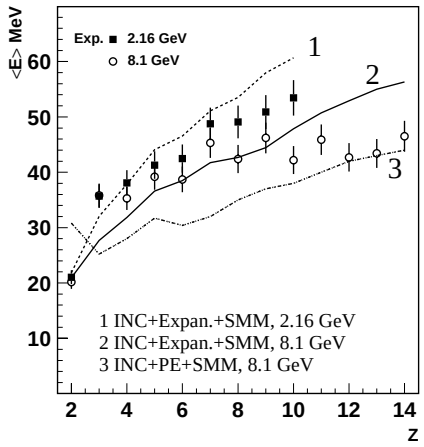

Fig. 9. Mean kinetic energies of fragments in p + Au collisions at 2.16 GeV (solid points, line 1) and 8.1 GeV (open points, lines 2,3). The lines are calculated with modified INC+Expansion+SMM(1,2) and INC+PE+SMM(3)

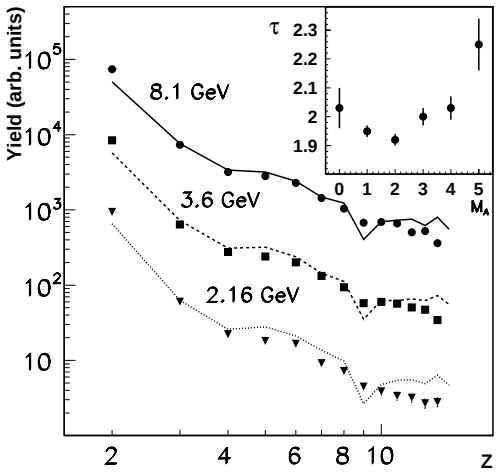

Fig. 10. Fragment charge distributions at the beam energies 8.1 GeV (top), 3.6 GeV (scaled by 1/4) and 2.16 GeV (scaled by 1/16). The lines are calculated by INC+Expansion+SMM (normalized at Z=3). The insert gives the τ-parameter deduced from the IMF-charge spectra for the beam energy of 8.1 GeV as a function of the measured IMF multiplicity

ation. The SMM version used includes deexcitation only after the acceleration.

Figure 10 shows the charge distributions of IMFs. The cross section for IMF production at 8.1 GeV incident energy is estimated to $\approx$ 600 mb; at the lowest incident energy $\approx$ 240 mb. The calculations using the INC+-Expansion+SMM model agree quite well with the data describing a plateau for Z= 4 – 6. The dip at Z=4, according to SMM, is caused by the instability of ^{8}Be. The model slightly underestimates the yield of fluorine isotopes probably overestimating its secondary decay because of shell effects. The general trend of the distributions is often described by a power law $Y(Z) \sim Z^{-\tau}$ which is also successful in describing our data yielding $\tau = 2.17 \pm 0.08$, 1.90 ± 0.06 and 1.93 ± 0.06 for the incident energies of 2.16, 3.6 and 8.1 GeV. The charge distributions are further studied by selecting different IMF-multiplicity. The insert in Fig. 10 shows the dependence of the τ-parameter on the measured IMF-multiplicity M_A for the incident energy of 8.1 GeV. With increasing multiplicity, the τ-parameter first decreases and then rises. In earlier papers on multifragmentation [35,36] the power-law behaviour for the fragment charge yield and the observed minimum of the τ parameter was interpreted as an indication of the proximity to the critical point for the liquid-gas phase transition in nuclear matter. But in fact the fragmenting system is not so close to the critical point [37] and one should look for a less exotic explanation of the minimum found here for the τ parameter as a function of M_A. A convenient interpretation can be found in a careful study of the secondary decay of excited fragments. As already mentioned, the IMF multiplicity is correlated with the excitation energy of the system. For the low multiplicities the system is close to the evaporation regime. In this case increasing excitation energy results in enhancement of the yield of heavier fragments (τ decreases). As the excitation continues increasing, the secondary decay of the fragments becomes more significant, enhancing the yield of lighter fragments (τ rises) [38].

It was mentioned in the introduction that the IMF+IMF angular correlation gives important information on the emission time. The correlation function $R(\theta_{12})$ from the coincidences between the trigger telescopes and the PM's of the fragment multiplicity detector at the beam energy 8.1 GeV shows a minimum at $\theta_{12} \approx 0$ caused by the Coulomb repulsion between fragments. The magnitude of the small angle suppression is practically the same as for ^{4}He (14.6 GeV) + Au [16]. This means that the IMF emission time for proton-induced multifragmentation does not exceed 100 fm/c as it does for He+Au. Detailed analysis of the angular correlations will be presented in a separate publication.

4 Conclusion

Multiple emission of intermediate mass fragments has been studied for the p + Au at the beam energies 2.16, 3.6 and 8.1 GeV with the modified FASA setup. The mean IMF multiplicities for events with at least one IMF are equal to 1.7 ± 0.2, 1.9 ± 0.2 and 2.1 ± 0.2 respectively. The intranuclear cascade calculations followed by statistical fragmentation do not describe the measured decay properties of a target spectator for the projectile energies used. The experimental data on the IMF multiplicity and charge distributions as well as fragment kinetic energies are described only by modifying the distributions of excitation energy and residual masses (and charges). This change takes into account the mass and energy loss during the expansion phase. In earlier studies [15,16,23] we showed that fragment emission occurs from a diluted system and within a short time interval of < 100 fm/c. The measured energy spectra of the fragments are explained

by a thermal and Coulomb part; a contribution from a collective flow is negligible ($v_{flow} < 0.02$ c). It is shown that the IMF emission is isotropic in the frame of one single source. The dynamics leading to the break-up stage does apparently not manifest itself in the observed properties of IMF emission in the studied reaction. All these arguments together suggest that in the studied interaction of relativistic protons with gold the fragment emission is a new decay process, a thermal multifragmentation of a hot and expanded nuclear system.

The authors are thankful to Proffs. A. Hrynkiewicz, A.M. Baldin, S.T. Belyaev and E. Kankeleit for support. The research was supported in part by Grant No RFK300 from the International Science Foundation and Russian Government, Grant No 96–02–18952 from Russian Foundations for Basic Research, by Grant No 94–2249 from INTAS, by Grant No P30B 09509 from Polish State Committee for Scientific Research, by Contract No 06DA453 with Bundesministerium für Forschung und Technologie and by the US National Science Foundation.

References

1. W.G. Lynch, Ann. Rev. Nucl. Part. Sci. **37** (1987) 493
2. L.G. Moretto and G.J. Wozniak, Ann. Rev. Nucl.Part. Sci. **43** (1993) 37
3. J.P. Bondorf, A.S. Botvina, A.S. Iljinov, I.N. Mishustin, K. Sneppen, Phys. Reports **257** (1995) 133
4. J. Pochodzalla et al., Phys. Rev. Lett. **75** (1995) 1040
5. V.V. Avdeichikov et al., Yad. Fiz. **48** (1988) 1796
6. V. Lips et al., Phys. Rev. Lett. **72** (1994) 1604
7. L. Pienkovski et al., Phys. Lett. B**336** (1994) 147
8. K.B. Morley et al., Phys. Rev. C**54** (1996) 737
9. E.R. Foxford et al., Phys. Rev. C**54** (1996) 749
10. W.-C. Hsi et al., Phys. Rev. Lett. **79** (1997) 817
11. G. Wang et al., Phys. Rev. C**53** (1996) 1811
12. K.H. Tanaka et al., Nucl. Phys. A**583** (1995) 581
13. A. Schüttauf et al., Nucl. Phys. A**607** (1996) 457
14. O. Schapiro, D.H.E. Gross, Nucl. Phys. A**573** (1994) 143
15. V. Lips et al., Phys. Lett. B**338** (1994) 141
16. S.Y. Shmakov et al., Yad. Fiz. **58** (1995) 1735; (Phys. of Atomic Nucl. **58** (1995) 1635
17. S.P. Avdeyev et al., JINR Rapid Comm. **2**(82) (1997) 71
18. S.P. Avdeyev et al., Pribory i Tekhnika Eksper. **39** (1996) 7; (Instr. Exp. Techn. **39** (1996) 153)
19. S.P. Avdeyev et al., Nucl. Instrum. Meth. A**332** (1993) 149
20. D.W. Stracener et al., Nucl. Instrum. Meth. A**294** (1990) 485
21. V.D. Toneev, K.K. Gudima, Nucl. Phys. A**400** (1983) 173c
22. J. Bondorf et al., Nucl. Phys. A**444** (1985) 476; A.S. Botvina, A.S. Iljinov, I.N. Mishustin, Nucl. Phys. A**507** (1990) 649; A.S. Botvina et al., Phys. of Atomic Nuclei **57** (1994) 628
23. Bao-An Li, D.H.E. Gross, V. Lips and H. Oeschler, Phys. Lett. B**335** (1994) 1
24. M. Blann, Ann. Rev. Nucl. Sci. **25** (1975) 123
25. A.S. Botvina et al., Nucl. Phys. A**584** (1995) 737
26. W.A. Friedman, Phys. Rev. C**42** (1990) 667
27. G. Papp and W. Nörenberg, Heavy Ion Physics **1** (1995) 241; and to be published
28. Z.J. He, J.S. Wu and W. Nörenberg, Nucl. Phys. A**489** (1988) 421
29. W.A. Friedman and W.G. Lynch, Phys. Rev. C**28** (1983) 16
30. H.W. Barz et al., Nucl. Phys. A**561** (1993) 466
31. B.-A. Li et al., Phys. Lett. B**303** (1993) 225
32. A.M. Poskanzer, G.W. Butler and E.K. Hyde, Phys. Rev. C**3** (1971) 882
33. R. Trockel, Ph. D. thesis, University Heidelberg 1987
34. S.C. Jeong et al., Phys. Rev. Lett. **79** (1994) 3468; G.D. Kunde et al., Phys. Rev. Lett. **74** (1995) 38
35. A.S. Hirsch et al., Phys. Rev. C**29** (1984) 508
36. P.J. Siemens, Nature **305** (1983) 410
37. V.A. Karnaukhov, Yad. Fiz.(Phys. of Atomic Nuclei) **60** (1997) 1780
38. V.A. Karnaukhov et al., Dubna preprint E7-98-8